Jisha Joseph “Self-assembly of structurally diverse phosphomolybdates: synthesis, structure and properties.” Thesis. Research and Post gradute Department of Chemistry, St. Thomas college (autonomous), University of Calicut, 2020.

CHAPTER IV

Metal pyrazole complex incorporated PMO cluster based solids

Summary

The aggregation of phosphorous and molybdenum precursors in the presence of $MCl_2.xH_2O$ (M = Co, Ni, Cu and Zn) with pyrazole to form PMO cluster based solids of varying dimensionality is discussed in this chapter. The following solids were obtained under ambient conditions *viz.* $\{H(pz)\}_6\{Zn(pz)_4(H_2O)_2\}[\{Zn(pz)_2P_2Mo_5O_{23}\}_2].8H_2O$ (**7**), $[\{Cu(pz)_4\}_2\{H_2P_2Mo_5O_{23}\}].H_2O$ (**8**), $\{Ni(pz)_4\}[\{Ni(pz)_4\}_2\{H_2P_2Mo_5O_{23}\}]_2[\{Ni(pz)_4\}\{Ni(pz)_4(H_2O)\}\{HP_2Mo_5O_{23}\}]_2.14H_2O$ (**9**), $[Ni(pz)_4Cl_2]$ (**10**) and $\{pz\}_2[\{Co(pz)_4\}_5\{P_2Mo_5O_{23}\}_2].6H_2O$ (**11**). Under hydrothermal conditions, $[\{Cu(pz)_2\}_4\{CuMo_{12}O_{38}(OH)_2\}].8H_2O$ (**12**) was obtained. While, Solids **7-9** and **11** are Strandberg-type PMOs, **12** is a rare example of copper based Keggin cluster and **10** is merely a metal complex. The synthesized solids were characterized and their magnetic properties were investigated using Guoy Balance.

IV.1. Introduction

The role of organic ligands in the crystallization of PMO cluster based solids was explored in Chapters II and III. The ligands used were 2-amino-3-methyl pyridine (2*a*3*mp)*, 2-amino-4-methyl pyridine (2*a*4*mp*), benzimidazole (*bimi*), 4-aminopyridine (4-*ap)* and pyrazole (*pz*). It was observed that except *pz*, all other ligands exhibited poor complexation ability with zinc. Therefore, in this chapter an attempt has been made to synthesize PMO cluster based solids in the presence of metal chlorides and pyrazole. Pyrazole is well known in literature to form strong complexes with transition metals centers [1]. The previously reported pyrazole incorporated transition metal complexes (TMCs) with PMO cluster based solids have been summarized in Table IV.1.

In the present work, the synthesis was carried out at room temperature using solvent evaporation method and the following solids were obtained *viz.* $\{Hpz\}_6\{Zn(pz)_4(H_2O)_2\}[\{Zn(pz)_2P_2Mo_5O_{23}\}_2].8H_2O$ (**7**)**,** $[\{Cu(pz)_4\}_2\ \{H_2P_2Mo_5O_{23}\}].H_2O$ (**8**), $\{Ni(pz)_4\}[\{Ni(pz)_4\}_2\{H_2P_2Mo_5O_{23}\}]_2$ $[\{Ni(pz)_4\}\{Ni(pz)_4\ (H_2O)\}\ \{HP_2Mo_5O_{23}\}]_2.14H_2O$ (**9**), $[Ni(pz)_4Cl_2]$ (**10**) and $\{pz\}_2[\{Co(pz)_4\}_5\ \{P_2Mo_5O_{23}\}_2].6H_2O$ (**11**). A slight variation in the reaction parameters resulted in the formation of $[\{Cu(pz)_2\}_4\{CuMo_{12}O_{38}(OH)_2\}].8H_2O$ (**12**) under hydrothermal conditions. The incorporation of metal centers in PMO cluster based solids has a two-fold effect: (i) Firstly, it enables PMO clusters to form multi-dimensional solids (refer Table IV.2 for the classification) which as comparatively difficult to crystallize as compared to organically templated solids. Figure IV.1 provides a statistical analysis of TMC incorporated PMO cluster based solids reported in literature during the last two decades [2]. (ii) Secondly, presence of transition metal centers having unpaired electrons opens the possibility to

Table IV.1. Table summarizing pyrazole incorporated TMC in PMO cluster based solids reported in literature during the past decade.

Sl No.	Formula	Cell parameters	Synthesis	Class	Crystal structure description	Dimensi-onality	Ref.
1	[{Cu(*pz*)(H_2O)} {Cu(*pz*)$_3$(H_2O)} {Cu(*pz*)$_4$} {$P_2Mo_5O_{23}$}]	$P2_1/n$ *a*, Å =14.751(2) *b*, Å =21.635(3) *c*, Å =16.489(2) *β*, ° =110.343	Solvent evaporation technique Metal:Mo: ligand ratio is 1:3:1	I	{Cu^{II}(*pz*)$_3$(H_2O)O_2} and {Cu^{II}(*pz*)(H_2O)O_3} complex units covalently link adjacent {P_2Mo_5} clusters into linear chains ; each cluster is also capped by {Cu^{II}(*pz*)$_4$O} square pyramids	1-D	[3]
2	{Cu(*pz*)$_2$(H_2O)$_4$} [{Cu(*pz*)$_2$(H_2O)}$_2$ {Cu(*pz*)$_4$}$_2$ {$HP_2Mo_5O_{23}$}$_2$].6H_2O	$P\bar{1}$ *a*, Å =9.187(5) *b*, Å =12.409(7) *c*, Å =22.099(12) *α*, ° =90.640(10) *β*, ° =94.513(10) *γ*, ° =95.490(10)	Solvent evaporation technique Metal:Mo: ligand ratio is 1:3:2	I	The octahedral {Cu(*pz*)$_4$$O_2$} and the trigonal bipyramidal {Cu(*pz*)$_2$(H_2O)O_2} link the {P_2Mo_5} clusters into a 2-D sheet. A third complex unit, {Cu^{II}(*pz*)$_2$(H_2O)$_4$} occurs in between the sheets as counter cation	2-D	[3]
3	[{Cu(*pz*)$_4$}$_3$ {Cu(*pz*)$_3$ (H_2O)}$_2$ {$HP_2Mo_5O_{23}$}$_2$].9H_2O	$P\bar{1}$ *a*, Å =12.5446(9) *b*, Å =15.4392(12) *c*, Å =15.9536(12) *α*° =94.7020(10) *β*° =95.5840(10) *γ*° =100.2570(20)	Solvent evaporation technique Metal:Mo: ligand ratio is 1:3:3	I	The octahedral units {Cu^{II}(*pz*)$_4$$O_2$} covalently link neighboring {P_2Mo_5} clusters to form 1-D chain; two such chains are brought together by a second octahedral {Cu^{II}(*pz*)$_4$$O_2$} unit to form a double chain. Square pyramidal {Cu(*pz*)$_3$(H_2O)O} caps the double chains through oxygen of the phosphate group	1-D	[3]

4	$[\{Cu(pz)_4\}_2\{H_2P_2Mo_5O_{23}\}].H_2O$	*P*cca *a*, Å =16.1420(10) *b*, Å =13.9222(8) *c*, Å =23.3927(14)	Solvent evaporation technique Metal:Mo: ligand ratio is 1:3:4	I	$\{P_2Mo_5\}$ cluster is linked to four octahedral copper units $\{Cu^{II}(pz)_4O_2\}$	3-D	[3]
5	$(pz)_2[\{Co(pz)_4\}_5\{P_2Mo_5O_{23}\}_2].6H_2O$	$P2_1/c$ *a*, Å =22.081(3) *b*, Å =18.644(2) *c*, Å =16.078(2) *β*, ° =109.137(2)	Hydrother-mal synthesis Metal:Mo: ligand ratio is 1:3:6	I	Out of three cobalt octahedral $\{Co^{II}(pz)_4O_2\}$ complexes, two covalently link $\{P_2Mo_5\}$ clusters into 2-D sheets and the third one connect the sheets to form a double sheet	2-D	[4]
6	$(pz)\{Ni(pz)_4(H_2O)_2\}[\{Ni(pz)_4\}_5\{P_2Mo_5O_{23}\}_2].2H_2O$	$P2_1/c$ *a*, Å =24.674(3) *b*, Å =18.137(2) *c*, Å =16.223(2) *β*, ° =95.495(2)	Hydrother-mal synthesis Metal:Mo: ligand ratio is 1:3:6	I	Two octahedral Ni-*pz* complexes covalently link $\{P_2Mo_5\}$ clusters into 2-D sheets and the third one connects the sheets to form a double sheet. $\{Ni(pz)_4(H_2O)_2\}$ units occur in between the double sheets as counter cations	2D	[4]
7	$\{Cu(pz)_4(H_2O)_2\}[\{Cu(pz)_4\}\{Cu(pz)_4(H_2O)\}\{P_2Mo_5O_{23}\}].2H_2O$	$P\bar{1}$ *a*, Å =12.302(3) *b*, Å =14.192(4) *c*, Å =19.351(5) *α*, ° =97.761(5) *β*, ° =97.555(4) *γ*, ° =98.569(5)	Hydrother-mal synthesis Metal:Mo: ligand ratio is 1:3:6	I	Two asymmetric octahedral $\{Cu(pz)_4O_2\}$complexes link $\{P_2Mo_5\}$ clusters into double chain which is capped by a third octahedral $\{Cu(pz)_4(H_2O)O\}$ unit	2-D	[4]
8	$(pz)[\{Zn(pz)_3\}_3\{P_2Mo_5O_{23}\}].2H_2O$	$P2_12_12_1$ *a*, Å =15.516(3) *b*, Å =17.373(3) *c*, Å =21.437(4)	Hydrother-mal synthesis Metal:Mo: ligand ratio is	I	$\{P_2Mo_5\}$ cluster is linked to four trigonal pyramidal zinc units $\{Zn(pz)_3O_2\}$and one tetrahedral $\{Zn(pz)_3O\}$unit to	3-D	[4]

			1:3:6		form a 3-D framework		
9	$[Ag(pz)_2]_6[PMo_{12}O_{40}]_2.3H_2O$	R-3 *a*, Å =20.437(2) *c*, Å =48.003(1)	Hydrother-mal synthesis Metal:Mo: ligand ratio is 2:1:2	II	Two crystallographically independent $[PMo_{12}O_{40}]^{3-}$ clusters are arranged in an AB-AB mode to give two kinds of supramolecular layers. The layers are further connected by $[Ag(pz)_2]^+$ linkers to form complex 3-D supramolecular network	3-D	[5]
10	$[Ag(pz)_2]_3[PMo_{12}O_{40}]$	$P\bar{1}$ *a*, Å = 11.3185(17) *b*, Å = 11.3221(18) *c*, Å = 12.9277(19) *α*, ° = 113.086(2) *β*, ° = 113.086(2) *γ*, ° = 103.579(2)	Hydrother-mal synthesis Metal:Mo: ligand ratio is 8:1:12	I	Four-supporting $[PMo_{12}O_{40}]^{3-}$ anions are fused by $[Ag(pz)_2]^+$ subunits to form a 1-D chain. Through weak interactions of Ag···O (3.091 Å) a 2-D supramolecular layer is constructed	2-D	[6]

Table IV.2. Classification of Solids **7,9** and **11**.

Sl. No.	Solid	Class	Dimensionality
1	$\{Hpz\}_6\{Zn(pz)_4(H_2O)_2\}[\{Zn(pz)_2P_2Mo_5O_{23}\}_2].8H_2O$, **7**	**Class I:** PMO clusters covalently linked by TMCs extending into multi-dimensions	1-D
2	$[\{Cu(pz)_4\}_2\{H_2P_2Mo_5O_{23}\}].H_2O$, **8**	**Class I:** PMO clusters covalently linked by TMCs extending into multi-dimensions	2-D
3	$\{Ni(pz)_4\}[\{Ni(pz)_4\}_2\{H_2P_2Mo_5O_{23}\}]_2[\{Ni(pz)_4\}\{Ni(pz)_4(H_2O)\}\{HP_2Mo_5O_{23}\}]_2.14H_2O$, **9**	**Class I:** PMO clusters covalently linked by TMCs extending into multi-dimensions	2-D
4	$\{pz\}_2[\{Co(pz)_4\}_5\{P_2Mo_5O_{23}\}_2].6H_2O$, **11**	**Class I:** PMO clusters covalently linked by TMCs extending into multi-dimensions	2-D

explore their magnetic properties as spin-spin interactions between metal centers can result in interesting magnetic behavior. Therefore, the magnetic behavior of Solids **8-11**, was investigated using Guoy Balance.

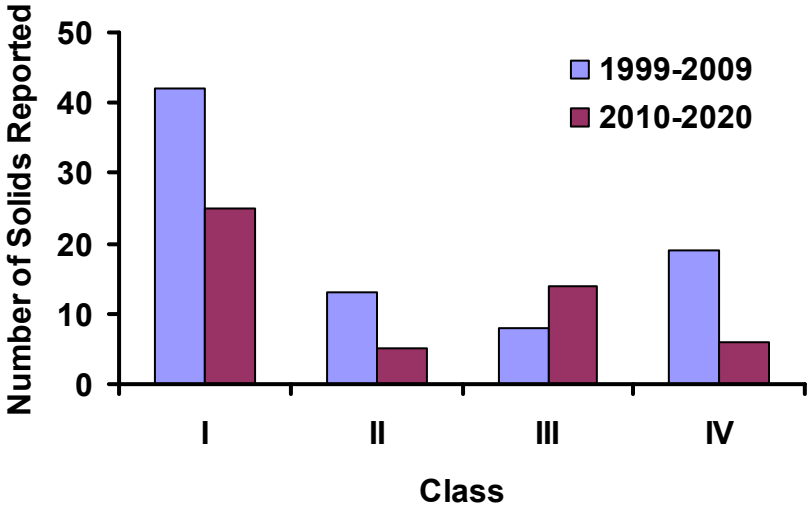

Figure IV.1. Statistical analysis of TMC incorporated PMO cluster based solids reported in literature during the last two decades.

[{Cu(*pz*)$_2$}$_4${CuMo$_{12}$O$_{38}$(OH)$_2$}].8H$_2$O (**12**) belongs to a unique class of polyoxometalates (POMs) called transition metal substituted POMs. This substitution can be of two types in Keggin polyanion, either by replacing the centre atom or one of the addenda atoms (refer Figure IV.2). Generally, the latter type of substitution is considered as a defect and the resultant product formed is named as lacunary POM. Only limited examples are reported in literature for copper substituted solids. The solid **12** draws special attention because only one solid is previously reported with copper as the centre of the Mo-O framework of Keggin type heteropolyanion. Zhang *et. al* synthesized [CuMo$_{12}$O$_{40}$]$^{6-}$ POM based MOF composite and studied its enhanced catalytic activities [7]. Two mono Cu(II) substituted phosphomolybdates [Cu$_4$(tea)$_6$(H$_4$PMo$_{11}$CuO$_{39}$)(PMo$_{12}$O$_{40}$)]$_2$.33H$_2$O and [Cu$_3$(tea)$_6$(H$_2$O)$_2$(H$_2$PMo$_{11}$CuO$_{39}$)$_2$]$_2$.30H$_2$O (tea =2-[1,2,4]triazol-4-yl-ethylamine) have

been reported by Tian *et. al*. in 2016 [8]. Properties of sodium and potassium salts of copper substituted Keggin type phosphomolybdates $Na_7PMo_{11}CuO_{40}$ and $K_5PMo_{11}CuO_{39}$ have also been investigated [9,10].

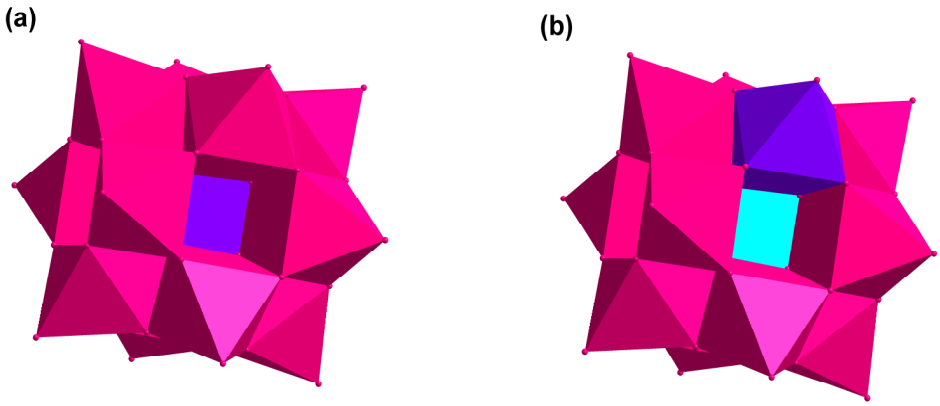

Figure IV.2. (a) Transition metal substituted Keggin type polyanion by replacing the central atom and (b) transition metal substituted Keggin type phosphomolybdate by replacing one of the addenda atoms.

IV.2. Experimental Section

IV.2.1. Synthesis

IV.2.1.1. Solvent evaporation method

Initially two different aqueous solutions were prepared. Solution A was prepared from metal chloride ($MCl_2.xH_2O$) and pyrazole (0.337 g, 4.95 mmol, Aldrich, 98%) in 20 ml of distilled water, while solution B was 20 ml of sodium molybdate solution ($Na_2MoO_4.2H_2O$, 0.2 g, 0.826 mmol, Merck, 99%). Solution B was added drop wise to solution A with constant stirring for 5-10 minutes. A precipitate was obtained upon stirring which was dissolved using 1M orthophosphoric acid (H_3PO_4, Merck, 85%). The resulting clear solutions were left

undisturbed for crystallization at room temperature. The resultant products were washed with water and acetone and allowed to dry in air. The experimental conditions have been summarized in Scheme IV.1.

IV.2.1.2. Hydrothermal synthesis

A mixture of metal chloride (MCl_2, 0.826 mmol, Aldrich, 98%), pyrazole (9.912 mmol, Aldrich, 98%) and sodium molybdate (0.826 mmol, Merck, 99%) was taken in 6 ml of distilled water, sealed in a 10 ml Teflon lined stainless steel container and heated at 180°C for 3 days. The initial pH was adjusted using 1 M orthophosphoric acid. After slow cooling to room temperature, the blue-black crystals were formed in the case of copper. The crystals were washed with water and acetone and allowed to dry in air. It is observed that except for $CuCl_2.2H_2O$, amorphous powder was obtained with other metal chlorides. The yield of **12** was found to be 70-75% based on Mo.

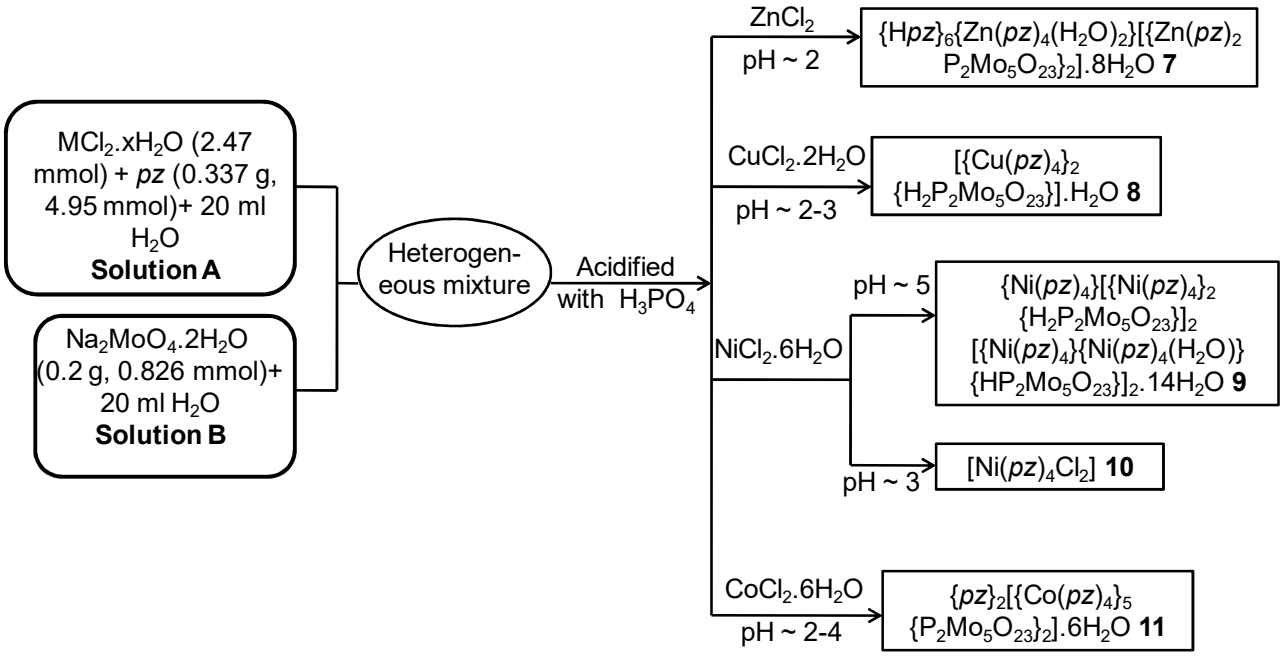

Scheme IV.1. Scheme showing the experimental procedure to crystallize solids **7-11**.

IV.2.2. Characterization

The solids were characterized using techniques discussed under Section II.2.2 in Chapter II. The crystal and refinement data for only solids **7, 9** and **12** have been summarized in Table IV.3 as details of solids **8**, **10** and **11** have already been reported in literature.

Table IV.3. Crystal and Refinement Data for Solids **7**, **9** and **12**.

	7	**9**	**12**
Formula	$C_{42}H_{64}Mo_{10}N_{28}O_{56}P_4Zn_3$	$C_{108}H_{146}Mo_{20}N_{72}Ni_9O_{108}P_8$	$C_{24}H_{32}Cu_5Mo_{12}N_{16}O_{48}P$
Formula weight, g	3136.66	6875.75	2845.69
T (K)	293(2)	293(2)	293(2)
Space Group	P -1	C2/c	P-1
a, Å	9.5647(15)	41.244(8)	12.727(2)
b, Å	12.558(2)	12.328(3)	13.165(2)
c, Å	20.340(3)	44.169(9)	13.882(2)
α, °	75.907(7)	90	66.680(3)
β, °	84.727(6)	91.62(3)	83.383(3)
γ,°	87.525(7)	90	65.274(3)
V, $Å^3$	2359.0(6)	22449(8)	1936.6(5)
Z	1	4	1
d_{calc}, $g \cdot cm^{-3}$	2.208	2.034	2.44
$\mu_{MoK\alpha}$, cm^{-1}	2.209	1.972	3.315
λ (Å)	0.71073	0.71073	0.71073
$R_1(I>2\sigma I)$, WR_2(all)	0.0590, 0.1491	0.0387, 0.0999	0.0782, 0.2165
GOF	1.063	1.116	1.107

IV.2.3. Magnetic susceptibility measurements

The magnetic moment and molar susceptibility are given by the following equations:

$$\text{Magnetic moment } (\mu) = 2.828 \sqrt{\chi_m} \times T$$

$$\chi_m = \chi_g \times \text{molecular weight}$$

$$\chi_g = \frac{C \times L \times (R-R_o)}{w \times 10^9}$$

where,

C	=	Calibration constant
L	=	length of sample
W	=	weight of sample
R	=	sample reading
R_o	=	Empty tube reading

IV.3. Results and discussion

The solids **7-9** and **11** are based on $\{P_2Mo_5\}$ cluster anion and its structure has been discussed under Section II.3 in Chapter II. Solid **12** is based on Keggin type polyanion [11, 12], in which copper atom is located at the inversion center. The CuO_4 tetrahedron is surrounded by four Mo_3O_{13} units formed by edge-sharing octahedral which are connected to each other by corner sharing oxygen atoms.

IV.3.1. Crystal structure of 7

In $\{Hpz\}_6\{Zn(pz)_4(H_2O)_2\}[\{Zn(pz)_2P_2Mo_5O_{23}\}_2].8H_2O$ (**7**) **,** the zinc complex, $\{Zn(pz)_2O_3\}$ derivatizes the $\{P_2Mo_5\}$ cluster through Zn–O coordination to form 1-D chains (refer Figure IV.3) which further aggregates through non-bonding interactions with octahedral $\{Zn(pz)_4(H_2O)_2\}^{2+}$ complex and six $(Hpz)^+$ cations to form 2-D sheets (Figure IV.4). The 3-D crystal packing is facilitated by CH…π interaction between neighboring sheets (Figure

IV.5). **7** is a new pseudopolymorph of $(pz)[\{Zn(pz)_3\}_3\{P_2Mo_5O_{23}\}].2H_2O$ reported by Thomas *et. al.* [4].

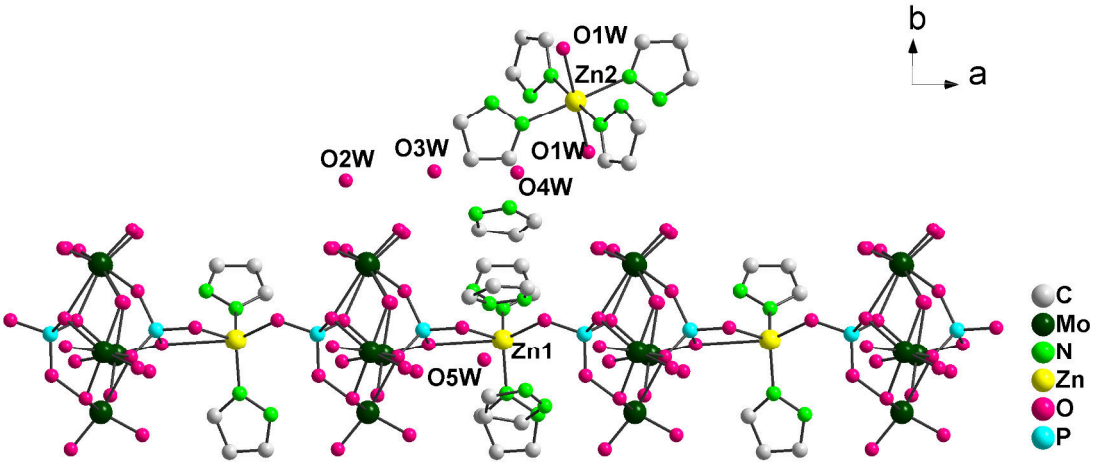

Figure IV.3. 1-D chains in **7**. H-atoms have been removed for clarity.

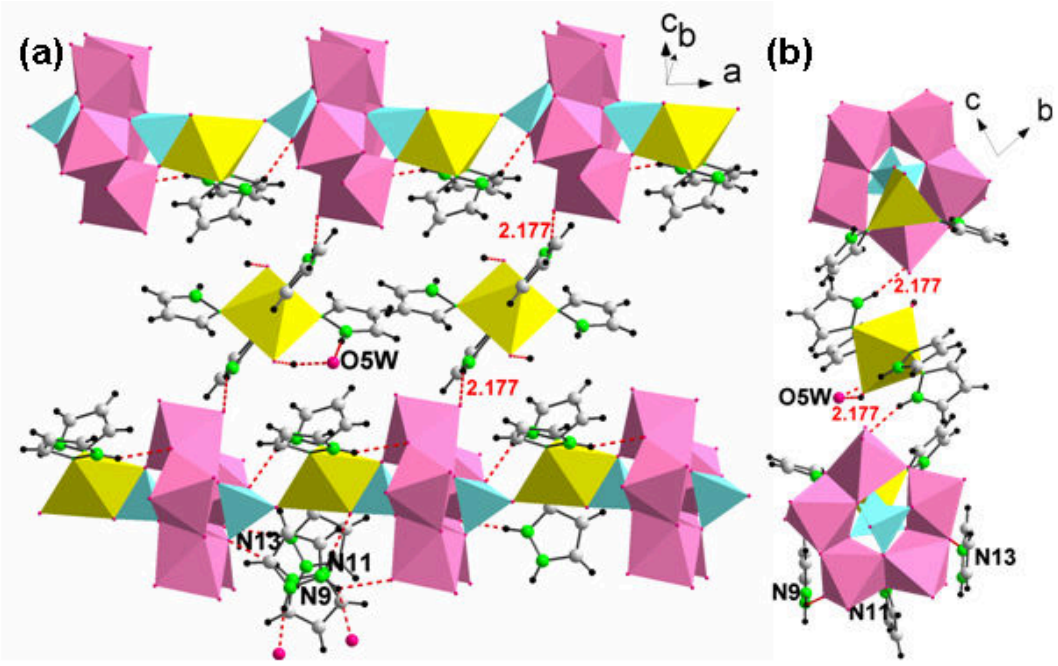

Figure IV.4. (a) Octahedral $\{Zn(pz)_4(H_2O)_2\}^{2+}$ complex links 1-D chains along with six $(Hpz)^+$ cations to form 2-D sheets (H-bonding interactions are shown in dashed red lines). (b) View along *a* axis.

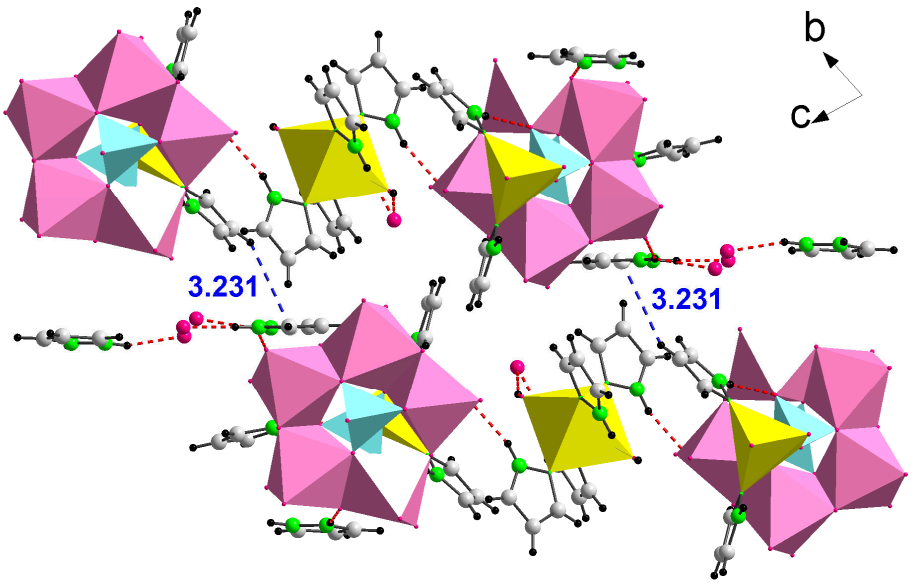

Figure IV.5. 3-D crystal packing is facilitated by CH…π interaction (shown in dashed blue lines) between neighboring sheets.

IV.3.2. Crystal structure of 8

The detailed crystal structure of $[\{Cu(pz)_4\}_2\{H_2P_2Mo_5O_{23}\}].H_2O$ (**8**) has already been reported by Thomas *et. al.* in 2008 [3]. The authors have reported that $\{P_2Mo_5\}$ cluster is linked to four octahedral copper units, $\{Cu^{II}(pz)_4O_2\}$ of which Cu2 covalently connects $\{P_2Mo_5\}$ clusters to form zig-zag chains which are further covalently linked by Cu1 complex to form a 3-D network (Figure IV.6).

IV.3.3. Crystal structure of 9

$\{Ni(pz)_4\}[\{Ni(pz)_4\}_2\{H_2P_2Mo_5O_{23}\}]_2$ $[\{Ni(pz)_4\}\{Ni(pz)_4(H_2O)\}\{HP_2Mo_5O_{23}\}]_2.14H_2O$ (**9**), is a novel polymeric solids in which the asymmetric unit consists of five nickel complexes and two $\{P_2Mo_5\}$ cluster anions as shown in Figure IV.7. Ni1 lies on inversion center which results in a tetrameric cluster unit as shown in Figure IV.7b. These units are connected Ni2

and Ni4 complexes to form a 2-D sheet. Of the lattice water molecules, only O2W is connected to Ni5 complex; remaining lattice water molecules occupy the voids in 2-D sheet. **9** is a new pseudopolymorph of $(pz)\{Ni(pz)_4(H_2O)_2\}[\{Ni(pz)_4\}_5\{P_2Mo_5O_{23}\}_2]\cdot 2H_2O$ reported by Thomas *et. al.* [4].

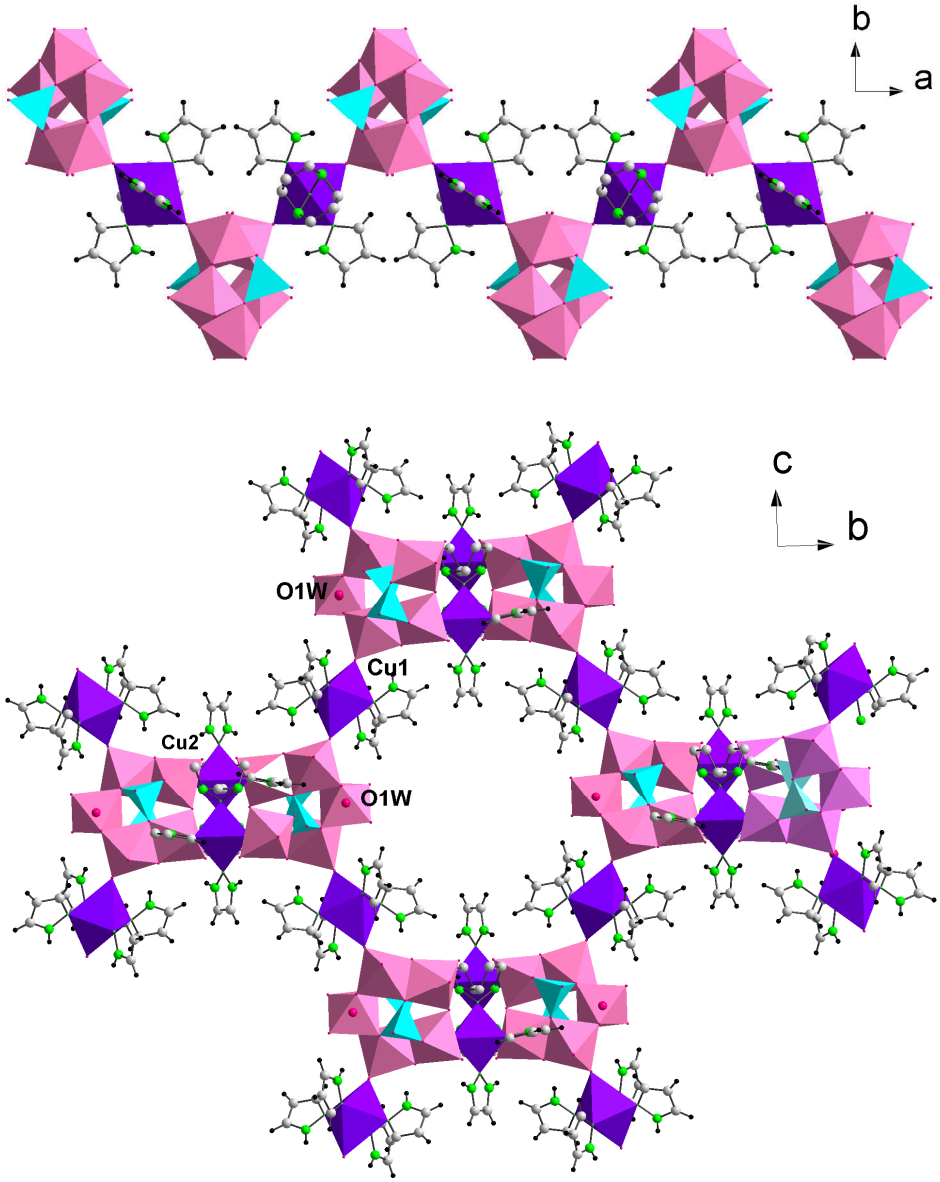

Figure IV.6. Zig-zag chains in **8** (top) connected by Cu1 to form 3-D structure of **8** (bottom).

IV.3.4. Crystal structure of 10

Crystal structure analysis of **10** showed that it is analogous to its cobalt and copper counterparts, reported in literature [13, 14]. In **10**, Ni center was coordinated to four *pz* units and two chlorine atoms to form an octahedral structure (refer Figure IV.8). The structure of $[Ni(pz)_4Cl_2]$ has been reported earlier by Reimann *et. al.* in 1967 [15].

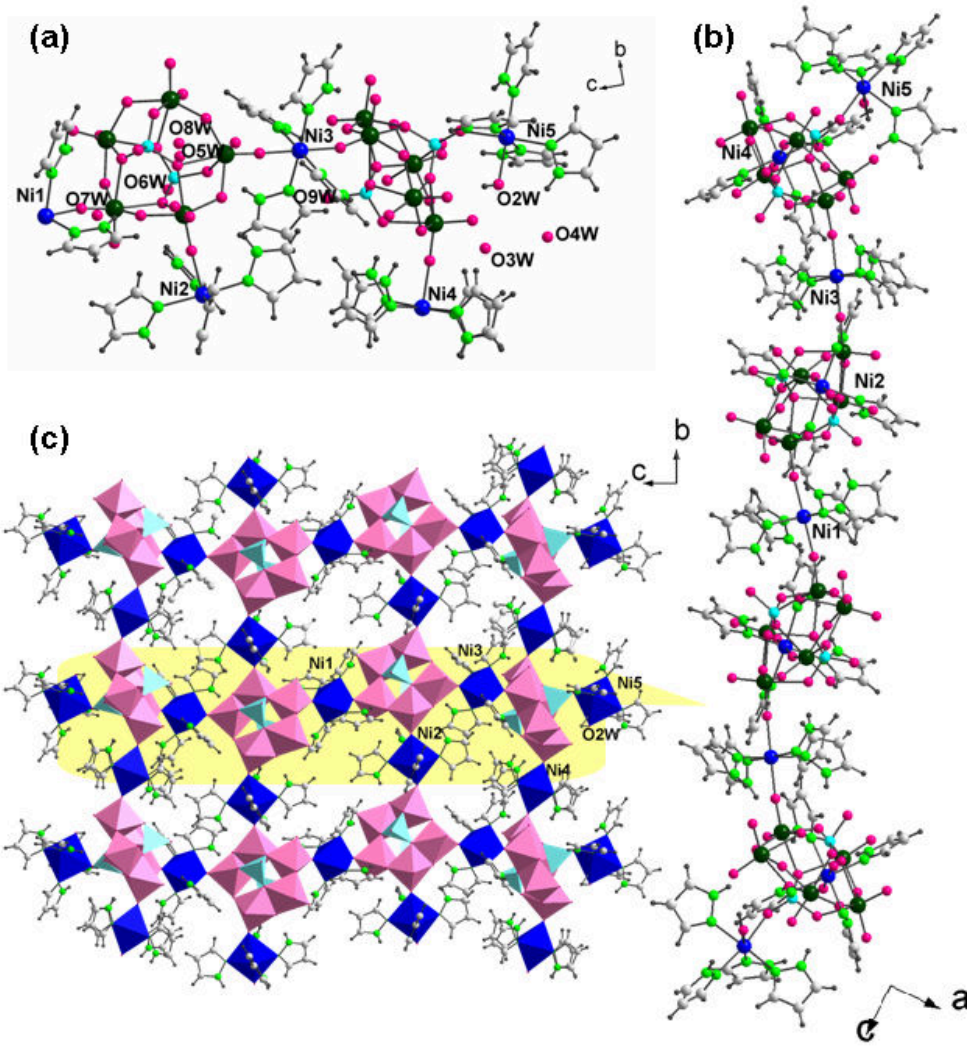

Figure IV.7. (a) Asymmetric unit in **9**. (b) Tetrameric cluster unit forming 2-D sheet as shown in (c). The lattice water molecules have been omitted for clarity.

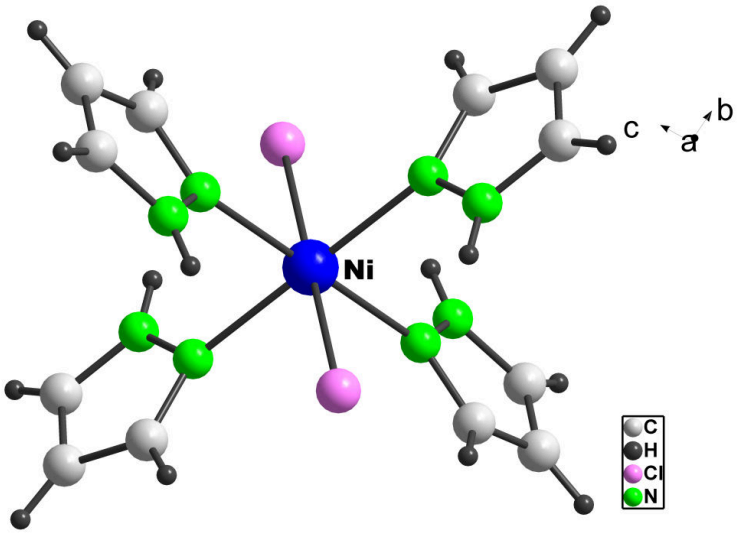

Figure IV.8. Six coordinated nickel complex of $[Ni(pz)_4Cl_2]$, **10**.

IV.3.5. Crystal structure of 11

The crystal structure of $\{pz\}_2[\{Co(pz)_4\}_5\ \{P_2Mo_5O_{23}\}_2].6H_2O$ (**11**) has been described earlier by Thomas *et. al.* in 2011 [4]. It was reported that "three sets of octahedral $\{Co^{II}(pz)_4O_2\}$ complexes (represented by three asymmetric cobalt, Co1, Co2 and Co3) are involved in the structure building. The Co1 and Co2 complex units covalently link $\{P_2Mo_5\}$ clusters into 2-D sheets and Co3 complex units connect the sheets to form a double sheet. The voids in the double sheets are occupied by free *pz* groups and the stacking of the double sheets along the *ab* plane is mediated by lattice water molecules present in the inter-lamellar region." (refer Figure IV.9).

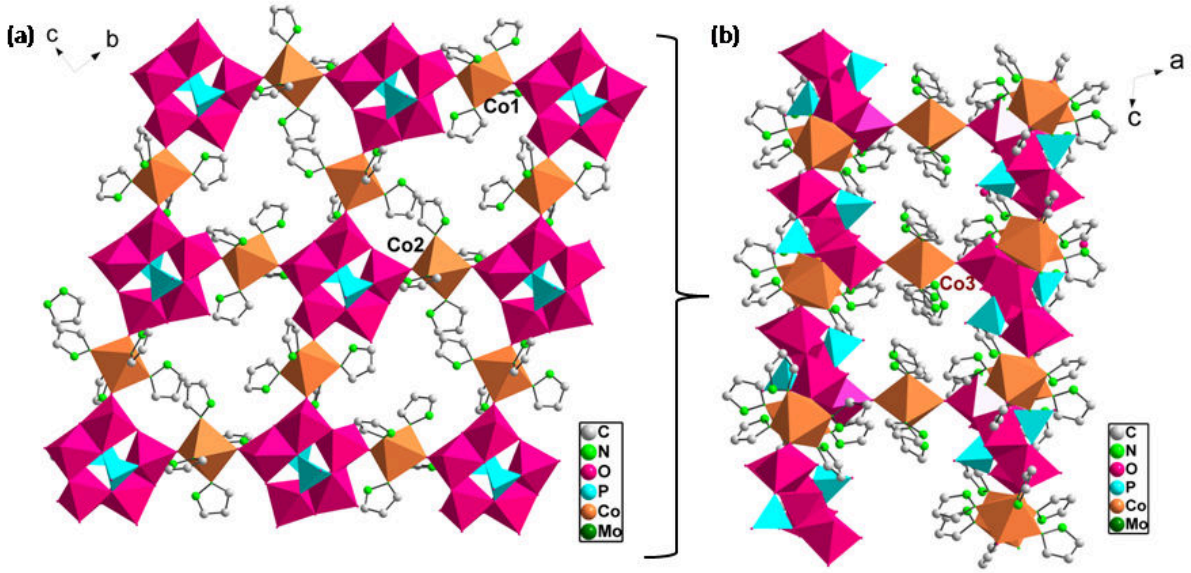

Figure IV.9. (a) Co1 and Co2 complex units covalently link $\{P_2Mo_5\}$ clusters into 2-D sheets. (b) Co3 complex units connect the sheets to form a double sheet. H atoms, free *pz* moieties and lattice water molecules have been omitted for clarity.

IV.3.6. Crystal structure of 12

The solid **12** is isostructural to $\{PMo_{12}O_{40}\}^{3-}$ Keggin type phosphomolybdate. However, instead of phosphorous, Copper is present at the inversion centre of the cluster framework of **12** (refer Figure IV.10). The BVS calculations [16] reveal that two terminal O6 atoms are protonated (refer Table IV.4). The cluster anions are covalently linked through Cu2 and Cu3 to form a 2-D sheet as shown in Figure IV.11. Among the eight lattice water molecules present, while O2W lies within the voids of the 2-D sheet; O1W, O3W and O4W formed a hexameric cluster which connects the two neighboring 2-D sheets (Figure IV.12).

Table IV.4. BVS calculations of **12**.

O—Mo	**Bond Length (Å)**		**BVS**	**O—Mo**	**Bond Length (Å)**		**BVS**
O1—Mo1	1.671(13)	1.892	1.892	O12—Cu1	1.502(18)	1.613	2.225
				O12—Mo1i	2.499(16)	0.202	
O2—Mo1	1.884(10)	1.064	2.059	O12—Mo3	2.475(16)	0.215	
O2—Mo4i	1.909(10)	0.995		O12—Mo4	2.511(14)	0.195	
O3—Mo1	1.918(12)	0.974	1.999	O14—Mo4	1.918(11)	0.971	2.055
O3—Mo2	1.898(15)	1.025		O14—Mo5	1.877(14)	1.084	
O4—Mo1	1.926(12)	0.95	1.955	O15—Mo4	1.912(13)	0.987	2.054
O4—Mo6	1.905(13)	1.005		O15—Mo6	1.883(15)	1.067	
O5—Mo1	1.891(9)	1.044	2.066	O16—Mo5	1.917(11)	0.973	1.904
O5—Mo3i	1.899(10)	1.022		O16—Mo2i	1.919(11)	0.931	
O6—Mo2	1.675(9)	1.872	1.872	O17—Mo5	1.663(10)	1.934	1.934
O7—Mo3	1.891(11)	1.044	2.083	O18—Mo5	1.870(14)	1.105	2.017
O7—Mo2	1.893(15)	1.039		O18—Mo3i	1.941(10)	0.912	
O8—Mo2	2.491(13)	0.206	2.164	O19—Mo5	1.894(11)	1.036	2.047
O8—Mo3	2.440(18)	0.237		O19—Mo6	1.903(10)	1.011	
O8—Cu1	1.524(14)	1.52					
O8—Mo5i	2.500(14)	0.201		O20—Mo6	1.665(9)	1.923	1.923
O9—Mo2	1.878(13)	1.082	2.085	O21—Cu1	1.554(15)	1.402	2.068
O9—Mo6	1.906(11)	1.003		O21—Mo2i	2.451(14)	0.23	
				O21—Mo6i	2.466(15)	0.221	
O10—Mo3	1.657(12)	1.965	1.965	O21—Mo1i	2.476(18)	0.215	
O11—Mo3	1.891(10)	1.044	2.052	O22—Cu1	1.550(14)	1.417	2.086
O11—Mo4	1.904(10)	1.008		O22—Mo4i	2.453(17)	0.229	
				O22—Mo5i	2.457(14)	0.226	
				O22—Mo6i	2.478(14)	0.214	

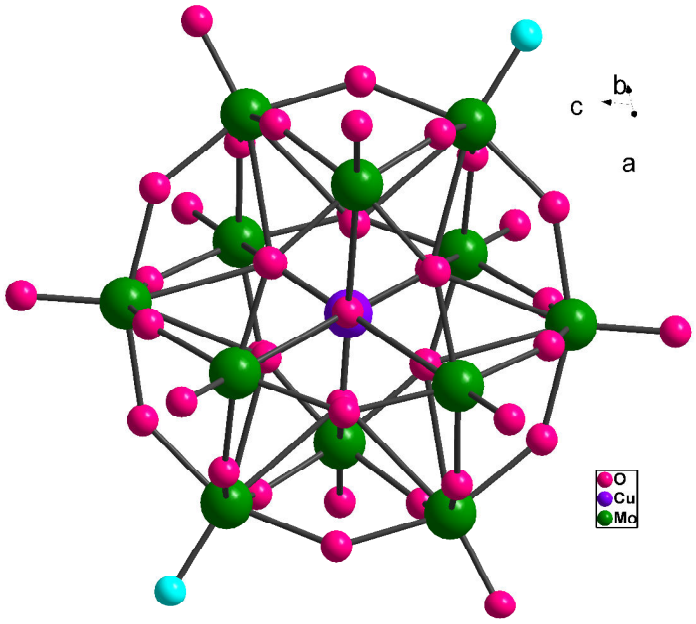

Figure IV.10. Keggin type polyanion which contains copper as the central atom. Two protonated terminal oxygen atoms (O6) are shown in cyan.

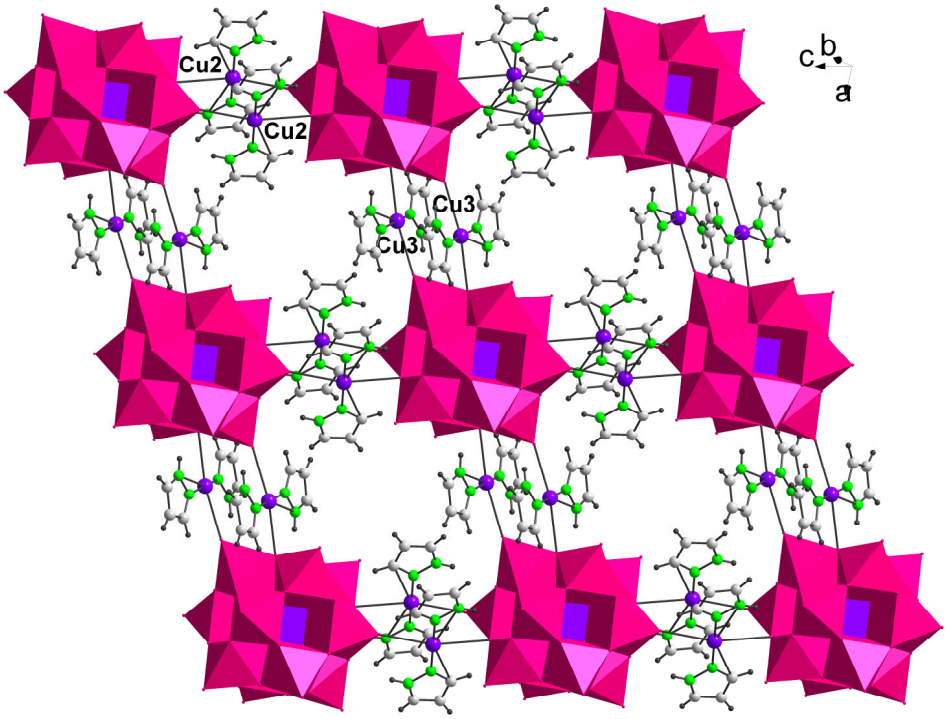

Figure IV.11. 2-D sheet formed connecting polyanions via copper- pyrazole complexes.

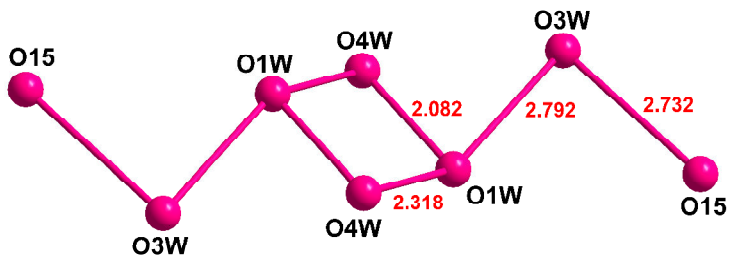

Figure IV.12. The hexameric water cluster in which the O…O interactions shown in solid lines.

IV.3.7. Analysis of solids 7 and 12

FTIR spectra of **7-11** shows the presence of characteristic P–O stretching and Mo–O stretching bands in the region 1000-1100 cm^{-1} and 640-930 cm^{-1} respectively. The finger print bands of Keggin type anions were observed in the region 700-1200 cm^{-1} for **12** [17-19]. The bands in the region 750-960 cm^{-1} could be attributed to Mo–O stretching vibrations. Broad band observed in solids **7-12**, in the region of ~ 3000-3500 cm^{-1} could be assigned to the stretching vibrations of O–H of water and N–H groups. (Figures IV.13-15).

The experimental and simulated powder X-ray pattern of solids **7-12** are given in Figures IV.16- IV.21. The comparison indicated that in all the cases, single phasic solids were obtained. The thermal degradation steps of TGA have been tabulated in Table IV.5 (also refer Figure IV. 22).

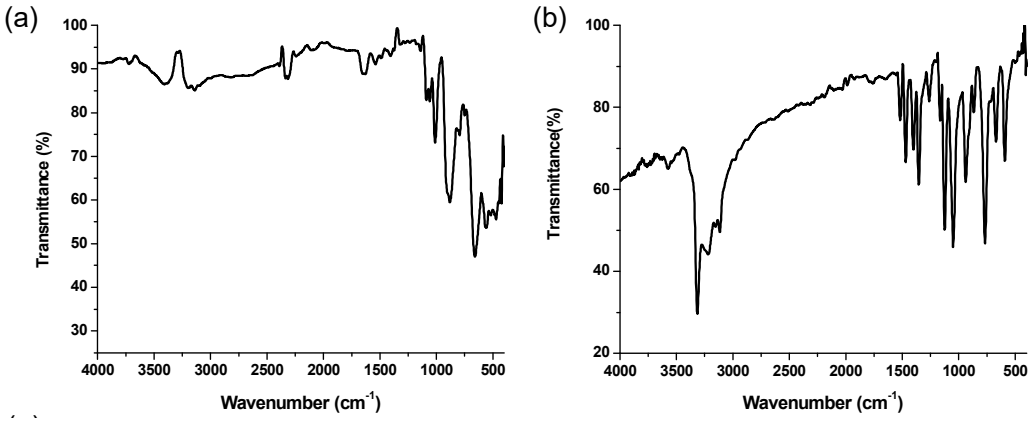

Figure IV.13. FTIR spectrum of (a) **7** and (b) **8**.

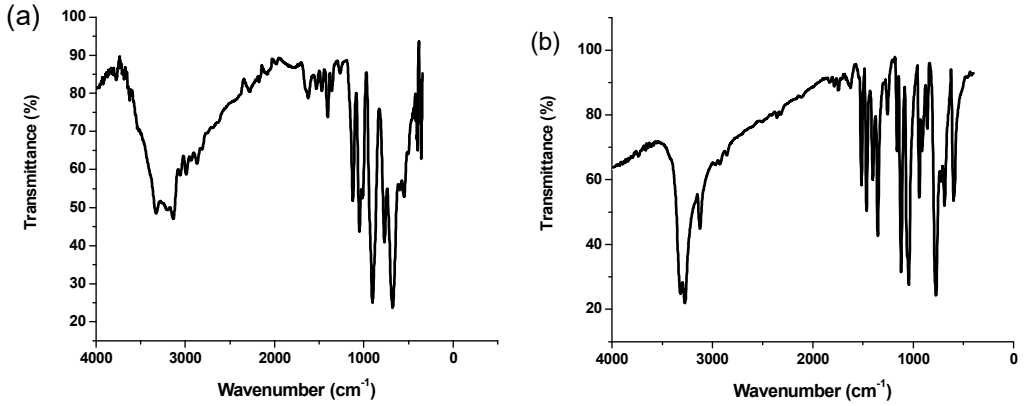

Figure IV.14. FTIR spectrum of (a) **9** and (b) **10**.

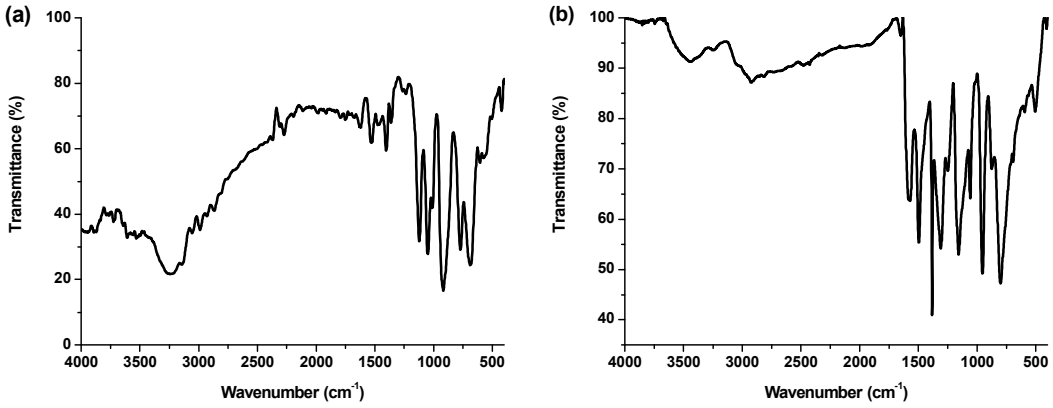

Figure IV.15. FTIR spectrum of (a) **11** and (b) **12**.

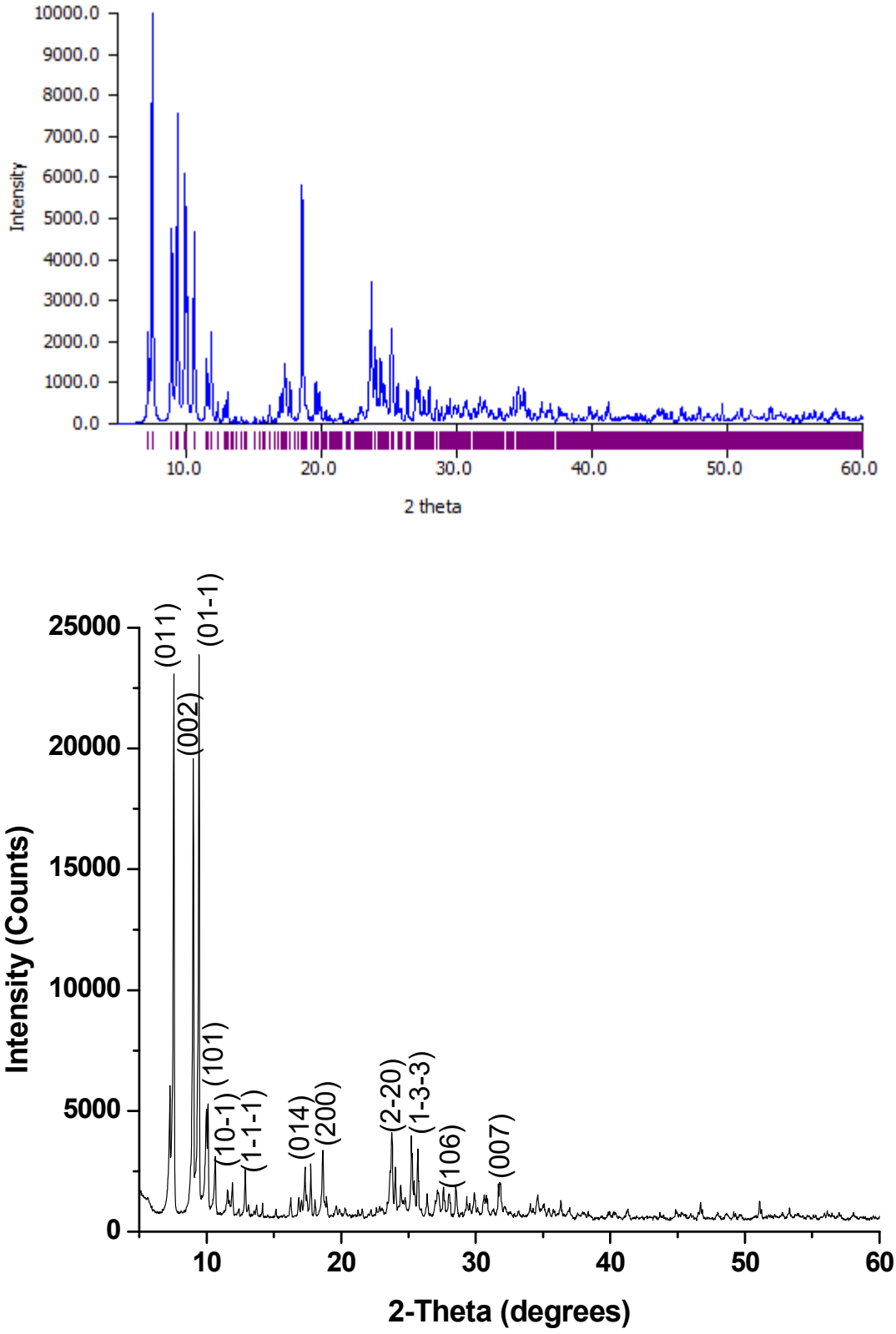

Figure IV.16. Simulated (top) and Experimental (bottom) PXRD of **7**.

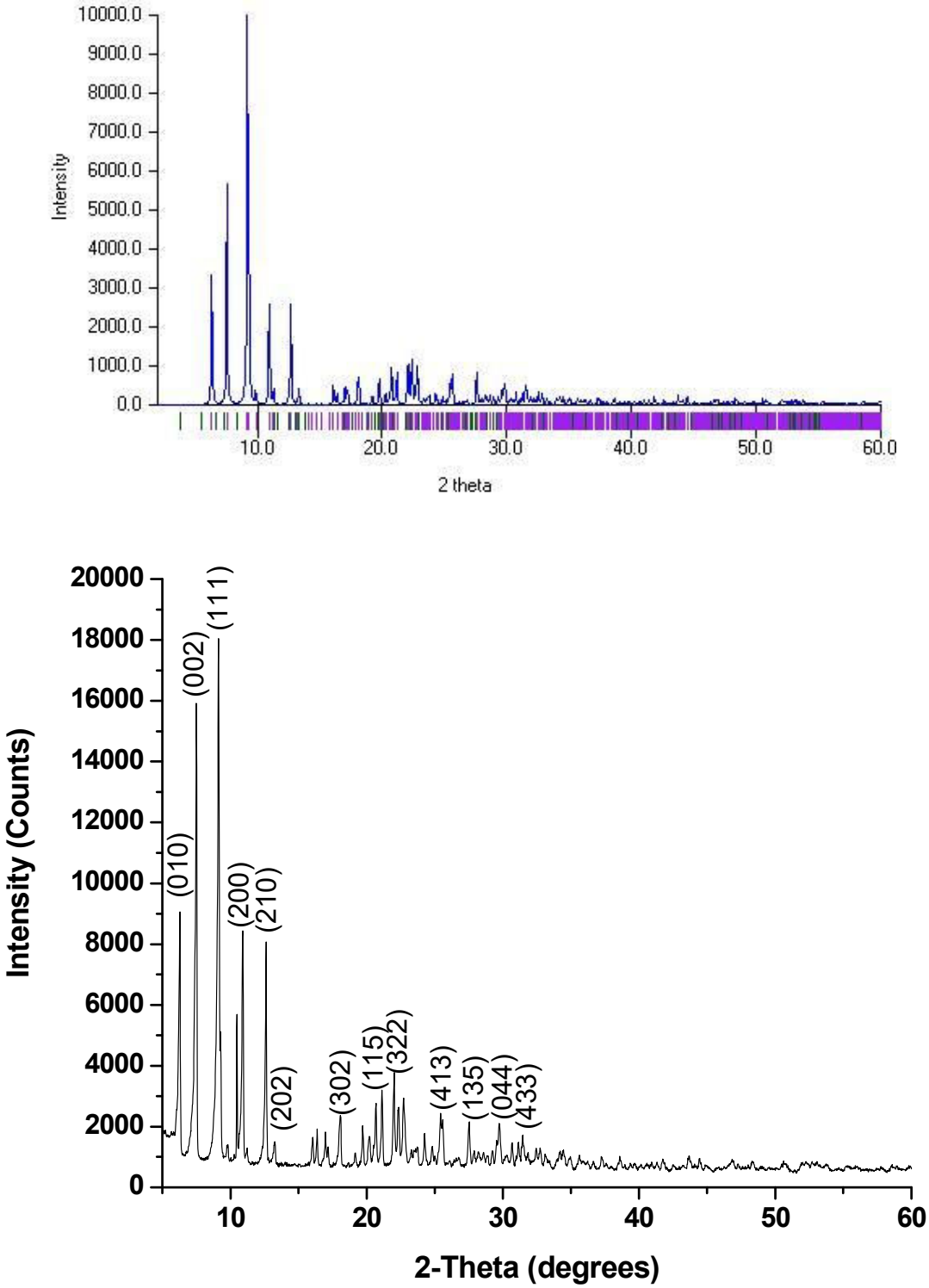

Figure IV.17. Simulated (top) and Experimental (bottom) PXRD of **8**.

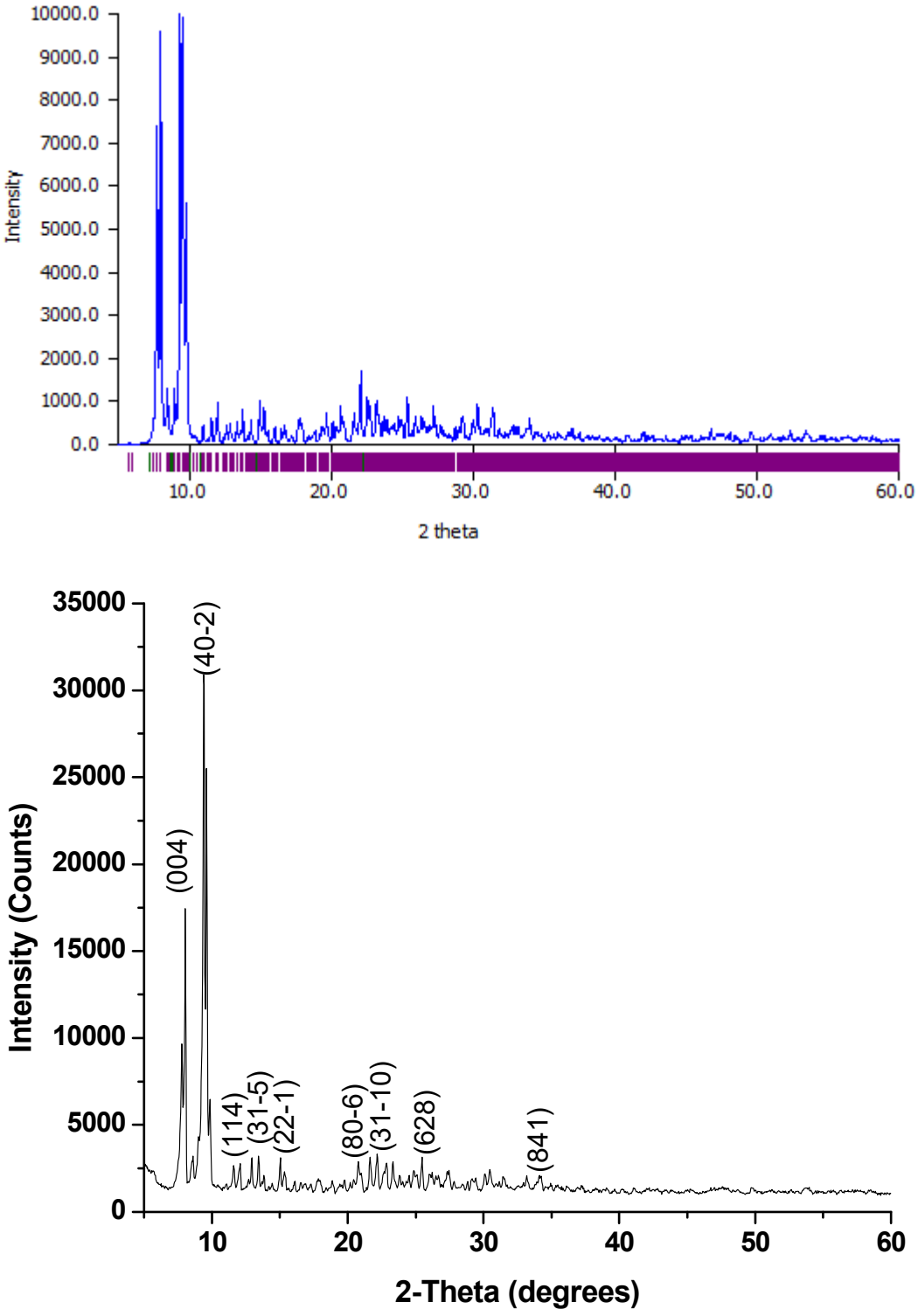

Figure IV.18. Simulated (top) and Experimental (bottom) PXRD of **9**.

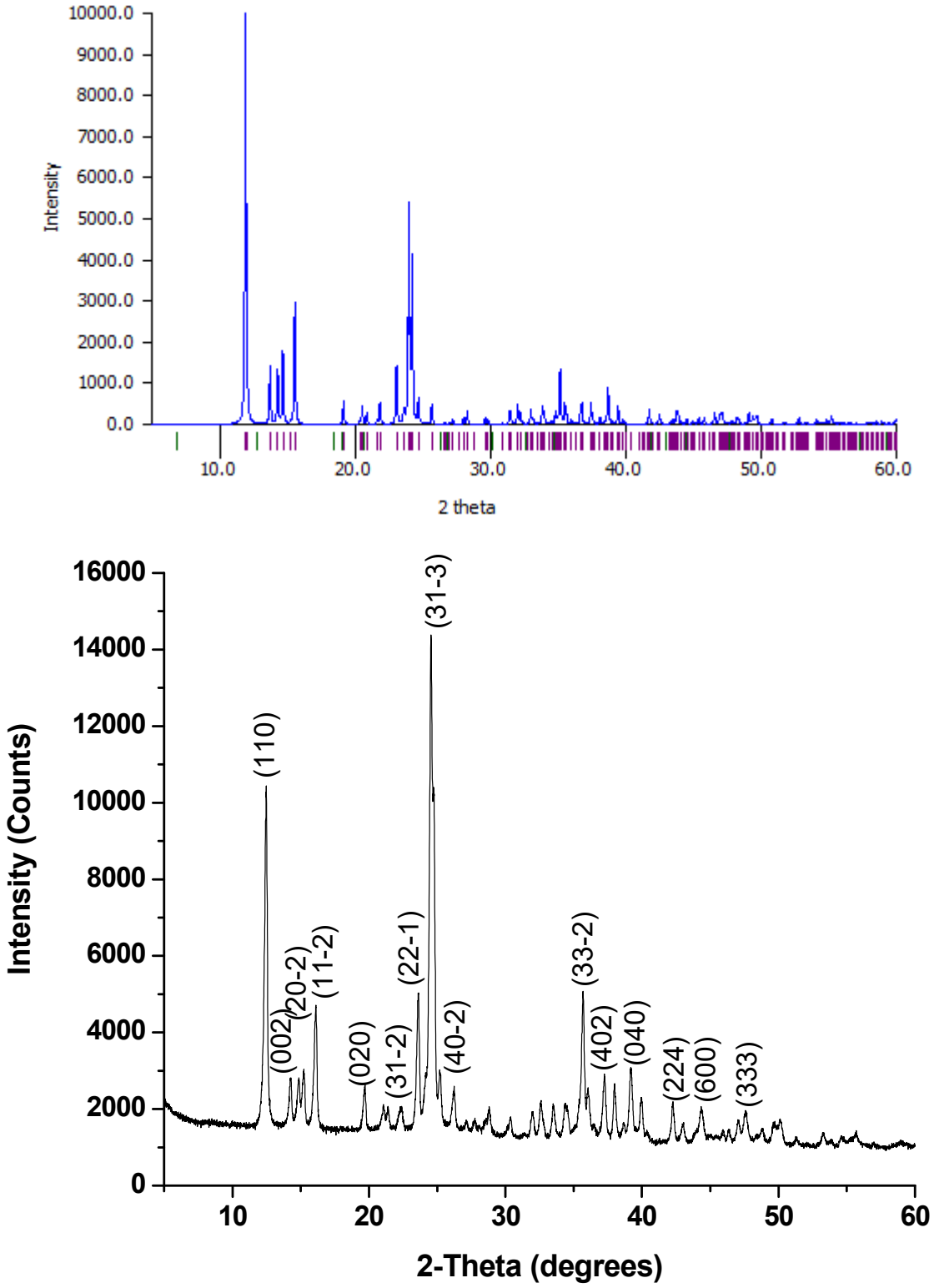

Figure IV.19. Simulated (top) and Experimental (bottom) PXRD of **10**.

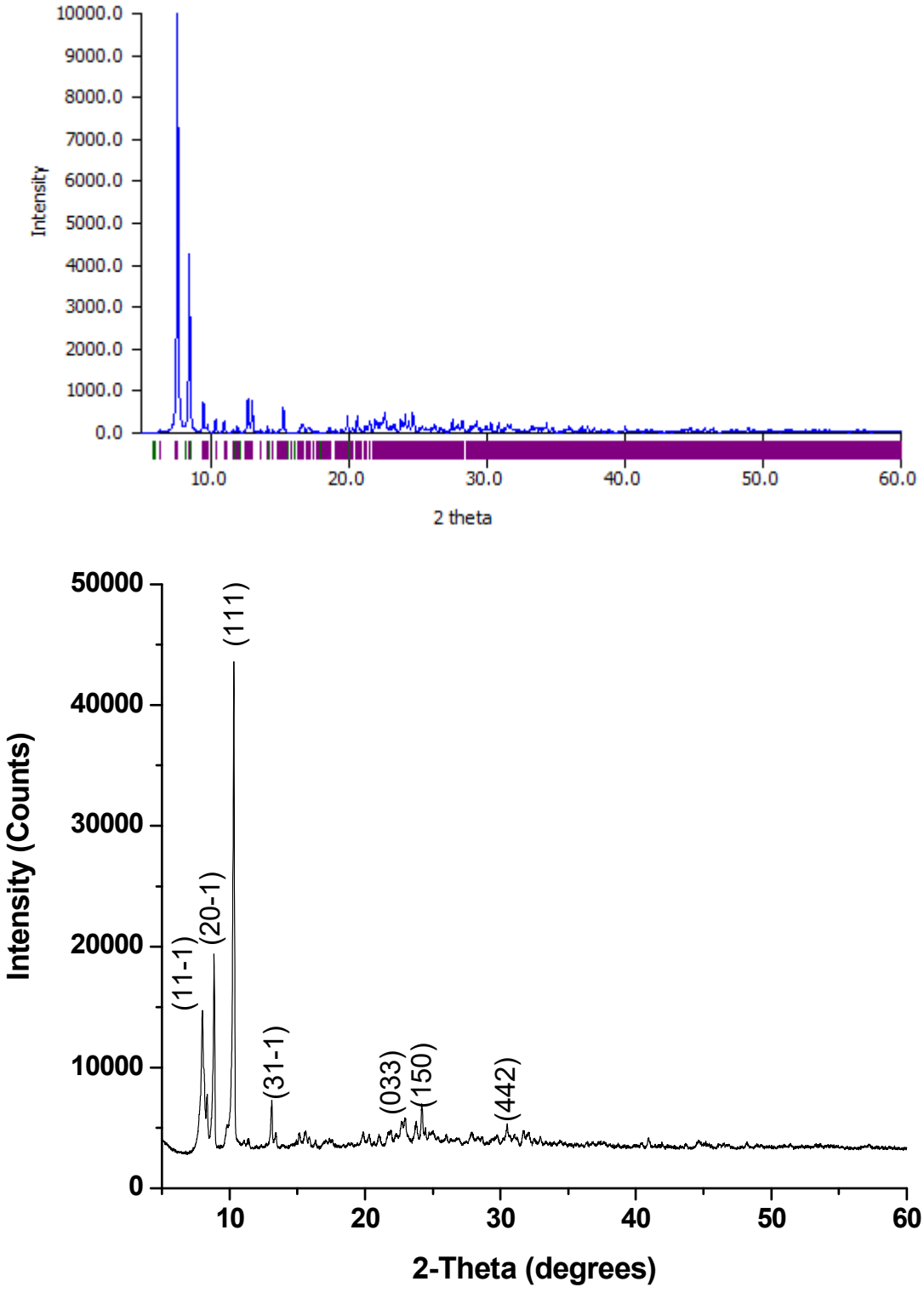

Figure IV.20. Simulated (top) and Experimental (bottom) PXRD of **11**.

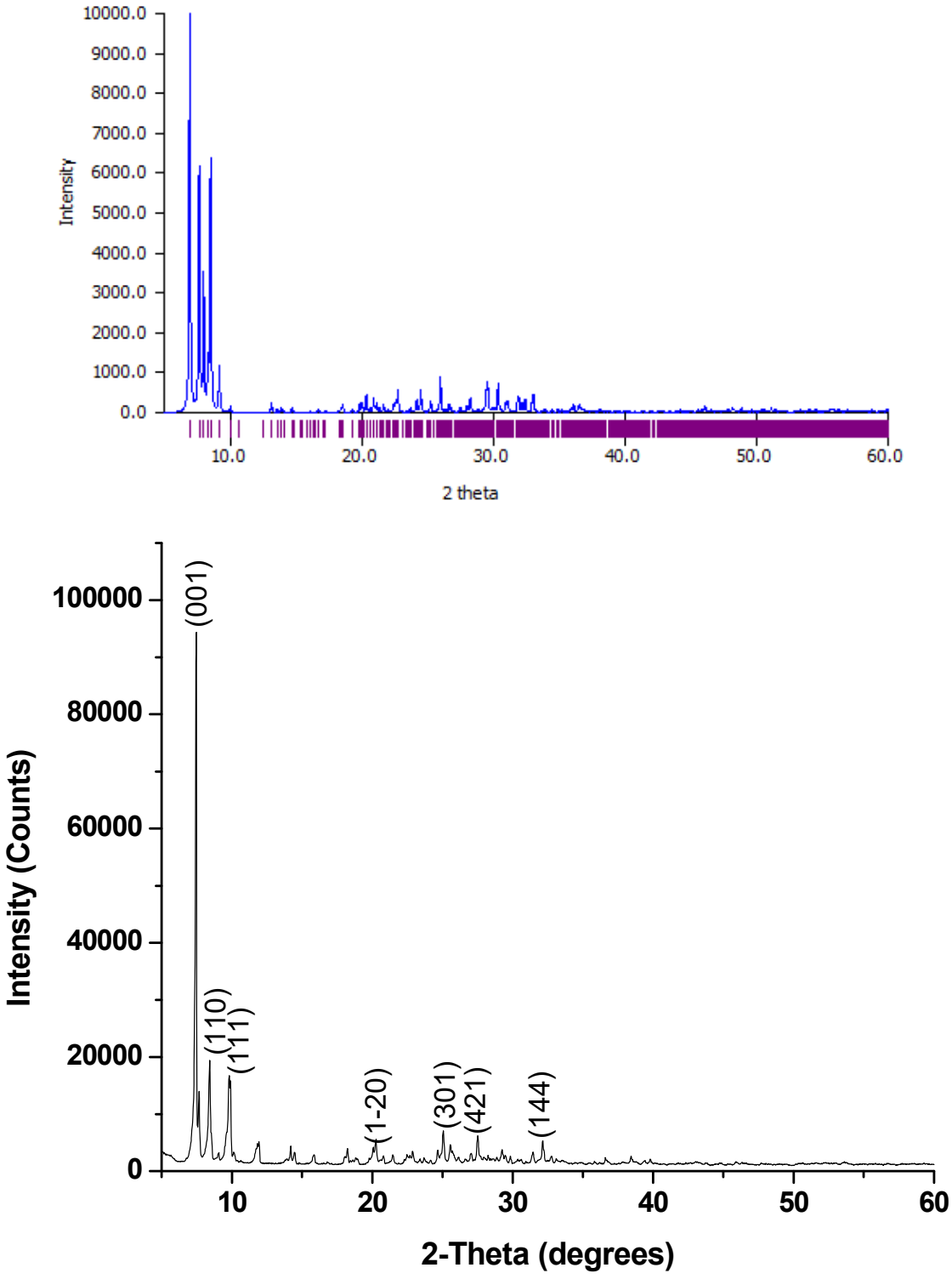

Figure IV.21. Simulated (top) and Experimental (bottom) PXRD of **12**.

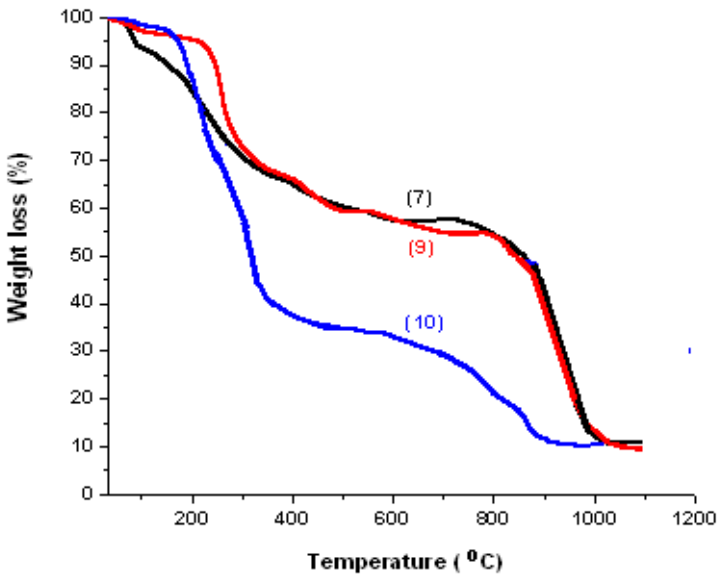

Figure IV.22. TGA of **7**, **9** and **10**.

Table IV.5. The summary of thermal degradation analysis of **7**, **9** and **10**.

Solid	Weight loss (%) TV= theoretical value	Temperature (°C)	Inference
7	~ 6 (TV = 4.5) ~37 (TV = 39.5)	Upto 100 Upto 625 Above 780	Loss of 8 H_2O molecules Decomposition of six H*pz* moieties + *pz* ligands coordinated to Zn ions Degradation of cluster anions
9	~ 3.5 (TV= 3.12) ~ 31.5 (TV = 30.3)	Upto 120 Upto 708 Above 850	Loss of 14 H_2O molecules Decomposition of *pz* ligands coordinated to Ni ions Degradation of remaining cluster unit
10	~ 1.5 ~ 84.6 (TV = 85.2)	100 Upto 853	Due to the moisture content of the solid surface Decomposition of two Cl and four *pz* ligands

IV.4. Magnetic properties

For solids **8-11**, the magnetic moment was calculated using spin only formula, $\mu = [n(n+2)]^{1/2}$ BM (where n is number of unpaired electrons).

In solid **8**, two copper centers are present and the observed magnetic moment obtained was 3.588. The calculated magnetic moment using spin only formula is 1.73. Therefore, the value obtained could be attributed to the contribution of two copper centers. In **10** which is a mere nickel complex, the calculated (2.82) and observed (2.84) values are in good agreement, confirming the presence of two unpaired electrons in the Ni center. However, in the case of **9** and **11**, the observed value showed a deviation from the calculated values. For **9**, the calculated and observed values are 2.82 and 10.799 respectively and for **11**, 3.87 and 11.738 respectively. Compared to the other solids, these solids have polymeric structures having more number of metal centers (9 Ni centers for **9** and 5 Co centers for **11**). Therefore, other parameters seem to be affecting the magnetic behavior of these two solids.

IV.5. Conclusions

The properties and dynamics of phosphomolybdates could be enhanced significantly by the incorporation of transition metal complexes. The association of ligands to the metal centers largely depends on the nature and pK_a value of the ligands used. In this chapter, *pz* has been selected on account of its coordination ability above pH 2.5. The pK_a value of pyrazole is 2.5 [4]. It can either be protonated or coordinated to a metal centre at acidic pH. So at pH ~2, *pz* existed in both forms: (*pz*) and $(Hpz)^+$ such as in $\{Hpz\}_6\{Zn(pz)_4(H_2O)_2\}[\{Zn(pz)_2P_2Mo_5O_{23}\}_2].8H_2O$ (**7**).

The ligand *pz* coordinated with Cu, Ni and Co in solids **8**-**12**, when the pH used was above 2.5. **7** and **9** are new pseudopolymorphs of solids $(pz)[\{Zn(pz)_3\}_3\{P_2Mo_5O_{23}\}]\cdot 2H_2O$ and $(pz)\{Ni(pz)_4(H_2O)_2\}[\{Ni(pz)_4\}_5\{P_2Mo_5O_{23}\}_2]\cdot 2H_2O$ respectively reported by Thomas *et. al.* [4] prepared under hydrothermal conditions. The results thus suggest that subtle changes in

reaction conditions can result in formation of new solids. On the other hand, crystallization of **8** and **11** using solvent evaporation method suggests that these solids have stable phases as they were also obtained earlier by Thomas *et. al.* under hydrothermal conditions [4]. Solid **12** is a peculiar one which has Keggin type polyanion, with copper at its centre in the place of phosphorous. It has also *pz* coordinated copper centers in its structure.

References

1. Crow, D. R.; Westwood, J. V. *J. Inorg. Nucl. Chem*. **1968**, 30, 179-187.
2. Thomas, J. Ph.D. Thesis, Indian Institute of Technology, Delhi, India, **2010**.
3. Thomas, J.; Ramanan, A. *Cryst. Growth Des*. **2008**, 8, 3390-3400.
4. Thomas, J.; Ramanan, A. *Inorg. Chim. Acta* **2011**, 372, 243-249.
5. Yu, K.; Zhou, B. *Z. Naturforsch., B: Chem. Sci*. **2015**, 70, 311-316.
6. Tian, A, X.; Tian, Y.; Ni, H. P.; Ji, X. B.; Ning, Y. L.; Hou, X. *J. Coord. Chem*. **2016**, 69, 2855-2863.
7. Zhang, J.; Zhang, J. *J. Clust. Sci*. **2020**, 31, 1051-1059.
8. Tian, A.; Ni, H.; Tian, Y.; Ji, X.; Liu, G.; Ying, J. *Inorg. Chem. Commun*. **2016**, 68, 50-55.
9. Xing, R.; Wang, F.; Dong, L.; Zheng, A. P.; Wang, L.; Su, W. J.; Lin, T.; *Food Chem*. **2016**, 197, 205-211.
10. Rezvani, M. A.; Shaterian, M.; Akbarzadeh, F.; Khandan, S. *Chem. Eng. J*. **2018**, 333, 537-544.
11. Liu, S.; Chen, L.; Wang, G.; Liu, J.; Gao, Y.; Li, C.; Shan, H. *J. Energy Chem*. **2016**, 25, 85-92.
12. Pathan, S.; Patel, A. *Catal. Sci. Technol*. **2014**, 4, 648-656.
13. Bagley, M. J.; Nicholls, D.; Warburton, B. A. *J. Chem. Soc. A*, **1970**, 2694-2697.
14. Xing, Y. H.; Han, J.; Zhang, B, L.; Zhang, X, J.; Zhang, Y. H.; Zhou, G. H. *Acta Crystallogr. Sect. E Struct. Rep. Online* **2006**, 62, m3354-m3356.
15. Reimann, C. W.; Mighell, A. D.; Mauer, F. A. Acta Cryst. **1967**, 23, 135-140.
16. Brown, I. D.; Altermatt, D. *Acta Crystallogr*. **1985**, B41, 244-247.

17. Ghalebi, H. R.; Aber, S.; Karimi, A. *J. Mol. Catal. A: Chem*. **2016**, 415, 96-103.

18. Tahar, A.; Benadji, S.; Mazari, T.; Dermeche, L.; Roch, C. M.; Rabia, C. *Catal. Lett*. **2015**, 145, 569-575.

19. Qi, M.; Yu, K.; Su, Z.; Wang, C.; Wang, C.; Zhou, B.; Zhu, C. *Inorg. Chim. Acta* **2013**, 400, 59-66.